JMB

RNA Chaperones Stimulate Formation and Yield of the U3 snoRNA–Pre-rRNA Duplexes Needed for Eukaryotic Ribosome Biogenesis

Tímea Gérczei[1,2], Binal N. Shah[1], Anthony J. Manzo[3], Nils G. Walter[3] and Carl C. Correll[1]*

[1]*Department of Biochemistry and Molecular Biology, Rosalind Franklin University of Medicine and Science, 3333 Green Bay Road, North Chicago, IL 60064, USA*

[2]*Department of Chemistry, Ball State University, Muncie, IN 47306, USA*

[3]*Department of Chemistry, University of Michigan, Ann Arbor, MI 48109-1055, USA*

Short duplexes between the U3 small nucleolar RNA and the precursor ribosomal RNA must form quickly and with high yield to satisfy the high demand for ribosome synthesis in rapidly growing eukaryotic cells. These interactions, designated the U3–ETS (external transcribed spacer) and U3–18S duplexes, are essential to initiate the processing of small subunit ribosomal RNA. Previously, we showed that duplexes corresponding to those in *Saccharomyces cerevisiae* are only observed *in vitro* after addition of one of two proteins: Imp3p or Imp4p. Here, we used fluorescence-based and other *in vitro* assays to determine whether these proteins possess RNA chaperone activities and to assess whether these activities are sufficient to satisfy the duplex yield and rate requirements expected *in vivo*. Assembly of both proteins with the U3 small nucleolar RNA into a chaperone complex destabilizes a U3 stem structure, apparently to expose its 18S base-pairing site. As a result, the chaperone complex accelerates formation of the U3–18S duplex from an undetectable rate to one comparable with the intrinsic rate observed for hybridizing short duplexes. The chaperone complex also stabilizes the U3–ETS duplex by 2.7 kcal/mol. These chaperone activities provide high U3–ETS duplex yield and rapid U3–18S duplex formation over a broad concentration range to help ensure that the U3–precursor ribosomal RNA interactions limit neither ribosome biogenesis nor rapid cell growth. The thermodynamic and kinetic framework used is general and thus suitable for investigating the mechanism of action of other RNA chaperones.

© 2009 Elsevier Ltd. All rights reserved.

Edited by J. Doudna

Introduction

RNA chaperones have long been recognized as proteins that help RNA trapped in a nonfunctional conformation to adopt its functional form by using such activities as RNA annealing, strand exchange, and duplex destabilization.[1] Activity is limited to aiding transitions not only from the "misfolded" form to the "folded" form but also from one functional form to another. Alternate RNA conformations often represent subsequent steps along a reaction pathway in such processes as pre-mRNA splicing and ribosome biogenesis. RNA chaperones are often obligatory when cellular demands dictate that these steps along the reaction pathway occur quickly and efficiently. To assess how these demands are met, we investigated how RNA chaperones mediate interactions between U3 small nucleolar RNA (snoRNA) and the precursor ribosomal RNA (pre-rRNA) in eukaryotic ribosome biogenesis (reviewed by Granneman and Baserga,[2] Henras *et al.*,[3] and Staley and Woolford[4]), a process essential

*Corresponding author. E-mail address: carl.correll@rosalindfranklin.edu.

Present address: T. Gérczei, Department of Chemistry, Ball State University, Muncie, IN 47306, USA.

Abbreviations used: snoRNA, small nucleolar RNA; pre-rRNA, precursor ribosomal RNA; SSU, small subunit; ETS, external transcribed spacer; FRET, fluorescence resonance energy transfer; ssFRET, steady-state FRET; Fl, fluorescein; Rh, tetramethylrhodamine; trFRET, time-resolved FRET; fwhm, full width at half-maximum.
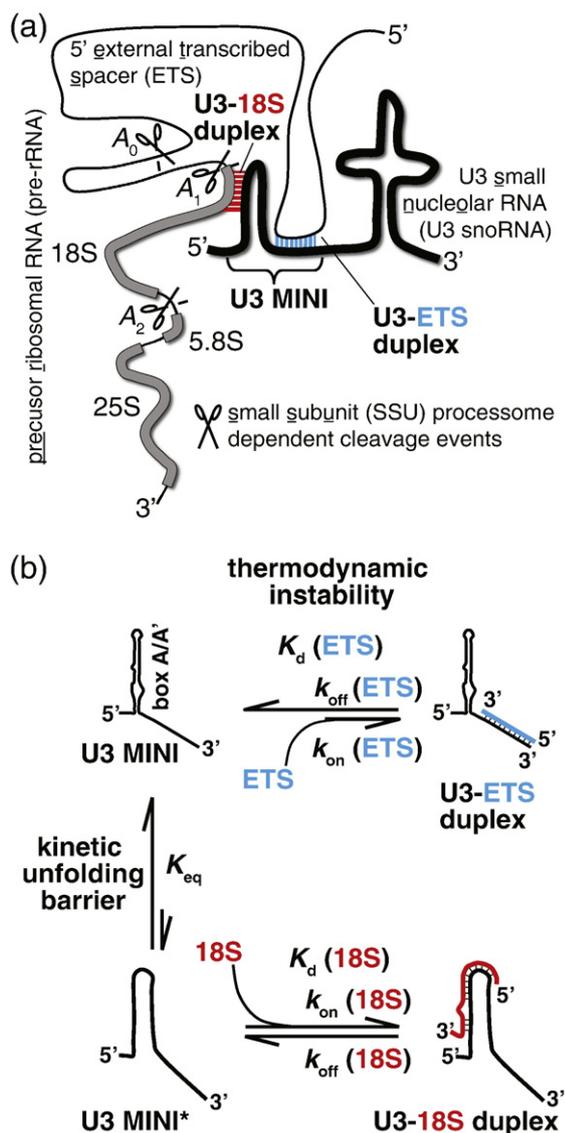
Fig. 1. A schematic view of U3–pre-rRNA interactions from *S. cerevisiae*. (a) The U3 snoRNA (thick black line) base pairs with the pre-rRNA that embeds three mature rRNAs (gray) between internal transcribed spacers and ETSs (thin line). Formation of the U3–ETS and U3–18S duplexes is a prerequisite for the U3-dependent cleavage events at A_0, A_1, and A_2. (b) Framework for formation of the U3–ETS and U3–18S duplexes with the minimal U3 binding site for Imp3p and Imp4p, U3 MINI. Duplex yield is limited by the thermodynamic instability of the U3–ETS duplex. Formation of the U3–18S duplex is hindered by a kinetic unfolding barrier; the box A/A′ stem structure of U3 MINI must open up to expose the base-pairing site. Thus, formation of the U3–18S duplex involves two steps: unfolding U3 MINI to U3 MINI* and hybridization. The duplex dissociation constant (K_d), duplex association and dissociation rate constants (k_{on} and k_{off}), and the equilibrium constant between U3 MINI and U3 MINI* (K_{eq}) are shown. The (ETS) or (18S) suffix is added to distinguish U3–ETS duplex parameters from those of the U3–18S duplex. Coloring of ETS (cyan) and 18S (red) sequences is used henceforth.

to cellular growth and linked to cancer (reviewed by Oskarsson and Trumpp[5]).

Fast and efficient initiation of small subunit (SSU) rRNA biogenesis is needed to supply the hundreds to thousands of ribosomes per minute required by rapidly growing eukaryotic cells. Formation of two short duplexes between the U3 snoRNA and the pre-rRNA, designated U3–ETS (external transcribed spacer) and U3–18S, is a prerequisite for the endonucleolytic cleavages that initiate SSU biogenesis.[6–11] These cleavages liberate the 18S precursor from the transcribed pre-rRNA, which embeds the 5.8S, 18S, and 25S–28S rRNAs between internal transcribed spacers and ETSs (Fig. 1).

Formation of both the U3–ETS and U3–18S duplexes docks the U3 snoRNA and its associated proteins, designated the SSU processome,[12–14] onto the pre-rRNA in a manner expected to recruit the as yet unidentified U3-dependent endoribonuclease(s) for cleavage at A_0, A_1, and A_2 (Fig. 1). Cleavage at A_2 releases the 18S precursor from the pre-rRNA and is observed by electron microscopy to occur during pre-rRNA transcription with an estimated half-life of 85 s *in vivo*.[15] As a prerequisite for cleavage, the U3–pre-rRNA duplexes are expected to form even faster. We also expect a high duplex yield (>90%) because duplex formation is essential for pre-rRNA processing and growth.[6–11]

RNA chaperones are needed to overcome two limitations to achieve sufficient duplex yield and formation rates (Fig. 1b). First, yield is limited by thermodynamic instability of the short U3–ETS duplex, made of only 10 base pairs. Second, a kinetic barrier limits formation of the other hybrid: the U3–18S duplex. Before the U3–18S duplex can form, the conserved box A/A′ stem structure must unfold to expose its base-pairing site. Formation of the U3–18S duplex thus occurs via two steps: unfolding and hybridization.

Previously, we showed with qualitative *in vitro* assays using minimal substrates[16] that the U3–18S and U3–ETS duplexes corresponding to those in *Saccharomyces cerevisiae* are observed only after addition of one of two proteins, Imp3p or Imp4p, presumably by overcoming these two limitations. Both proteins are part of the SSU processome, required for the U3-dependent cleavages and thus essential.[12,17] Our findings on these *S. cerevisiae* proteins are expected to apply to other eukaryotes because the pre-rRNA processing pathways, including the U3–pre-rRNA base-pairing potential,[18–20] and the associated *trans*-acting factors, including Imp3p and Imp4p, have counterparts in higher eukaryotes.[21]

Imp3p and Imp4p share the same minimal U3 binding site,[16] U3 MINI, raising the possibility that they assemble into a ternary complex. Does this ternary complex form? If so, does it possess chaperone activities sufficient to satisfy the *in vivo* requirements for rapid formation and high yield of the U3–pre-rRNA duplexes?

In this report, we address these questions by developing fluorescence-based and other assays to

ascertain the magnitude of the limits to U3–pre-rRNA yield and formation rate and the extent to which Imp3p and Imp4p overcome these limitations using minimal substrates. We demonstrate assembly of Imp3p, Imp4p, and U3 MINI into a ternary complex and show that it does not alter the association rate constant of either the U3–18S duplex or the U3–ETS duplex. Rather, assembly of the complex removes the kinetic unfolding barrier to expose the U3 MINI bases to permit apparently spontaneous formation of the U3–18S duplex. The assembled complex increases the stability of the U3–ETS duplex by 2.7 kcal/mol (20 °C), thereby increasing the yield of this short duplex. Estimates based on our findings show that activities of this assembly, designated the chaperone complex, are needed to satisfy the *in vivo* demands for rapid formation and high yield of the U3–pre-rRNA duplexes.

Results

Development of fluorescence resonance energy transfer-based assays

The distance-dependent nature of fluorescence resonance energy transfer (FRET) is ideally suited to monitor assembly of the chaperone complex and formation of the U3–18S and U3–ETS duplexes. In our steady-state FRET (ssFRET; i.e., with continuous illumination and observation) assays, one molecule is labeled with the donor fluorescein (Fl) and its potential partner is labeled with the acceptor tetramethylrhodamine (Rh). When partner macromolecules interact, they produce an ssFRET value above background if the fluorophore pairs are sufficiently close (between ∼15 and 80 Å). To confirm that the fluorescent labels do not interfere with binding activity, we determined that the RNA–protein K_d values using fluorescently labeled molecules (data not shown) were within a factor of 2 of those measured previously with radiolabeled RNA and unlabeled protein.[16] To determine the duplex association (k_{on}) and dissociation (k_{off}) rate constants, we monitored the signal change associated with the donor emission because it is larger than that of the acceptor emission. This phenomenon is due in part to FRET-independent cross talk from the donor to the acceptor than vice versa because of the asymmetry of their emission peaks.

Three lines of evidence provide confidence that the Fl signal monitors duplex formation in accord with FRET. First and foremost, addition of acceptor containing RNA molecules results in a decrease in the Fl peak emission with a concomitant increase in Rh peak emission for each case studied, whereas addition of an unlabeled partner to the Fl-labeled U3 MINI does not quench donor emission (Supplementary Fig. S1). Second, duplex k_{on} values were within a factor of 2 of those determined with fluorophores attached to different sites on the RNA substrates (data not shown). Third, the K_d calculated by dividing U3–18S duplex k_{off} by its corresponding k_{on} is within a factor of 2 of the mean K_d value measured by electrophoretic mobility shift assays (Table 1; Supplementary Fig. S2).

To distinguish the duplex parameters of the U3–ETS duplex from those of the U3–18S duplex, we henceforth designate the former k_{on} (ETS), k_{off} (ETS), and K_d (ETS) and the latter k_{on} (18S), k_{off} (18S), and K_d (18S).

Chaperone complex includes U3 MINI, Imp3p, and Imp4p

Our previous findings[16] showed that Imp3p and Imp4p share the same minimal RNA binding site, U3 MINI. To test whether these proteins assemble with U3 MINI into a ternary chaperone complex, we used ssFRET assays in which Fl-labeled Imp3p (Fl-Imp3p) contained the donor, Rh-labeled Imp4p (Rh-Imp4p) contained the acceptor, and U3 MINI was unlabeled (Fig. 2). Addition of Rh-Imp4p to a preformed binary complex of Fl-Imp3p and U3 MINI resulted in a FRET efficiency (E_{FRET}; calculated as described in Materials and Methods) value of 0.26±0.01, significantly above background (0.03), consistent with assembly (Fig. 2a, open bar). In contrast, only background E_{FRET} values were observed when Fl-Imp3p was added to either Rh-Imp4p (Fig. 2a, hashed bar) or a preformed binary complex of Rh-Imp4p and U3 MINI (Fig. 2a, black bar). Addition of unlabeled Imp4p to a preformed binary complex of Fl-Imp3p and U3 MINI showed no signal change and thus confirmed that the observed FRET signal results from the proximity of the Rh and Fl labels and not protein binding (Fig. 2b). These findings support the notion that an RNA-dependent chaperone complex assembles from U3 MINI, Imp3p, and Imp4p and lead to

Table 1. U3–18S duplex kinetic and thermodynamic parameters

| | MINI-17–18S | U3 MINI–18S | | | $\Delta\Delta G$ |
	No protein added	No protein added	Imp3p and Imp4p added	Fold change[a]	(kcal/mol)
k_{off} (18S)	$(1.0\pm0.1)\times10^{-4}$ s^{-1}	ND	$(2\pm1)\times10^{-3}$ s^{-1}	20-fold increase	1.7[b]
k_{on} (18S)	$(7\pm1)\times10^{5}$ M^{-1} s^{-1}	ND	$(7\pm1)\times10^{5}$ M^{-1} s^{-1}	No change	∼0
K_d (18S)	1.4×10^{-10} M^c	ND	$(4\pm2)\times10^{-9}$ M		

ND, not detectable.
[a] Fold change of U3–18S with protein to MINI-17–18S without protein.
[b] $\Delta\Delta G = -RT[ln(k_{off}$ (no protein added) for MINI-17–18S duplex$/k_{off}$ (protein added) for U3–18S duplex)] at 20 °C.
[c] Calculated from k_{off} (18S) and k_{on} (18S) values.
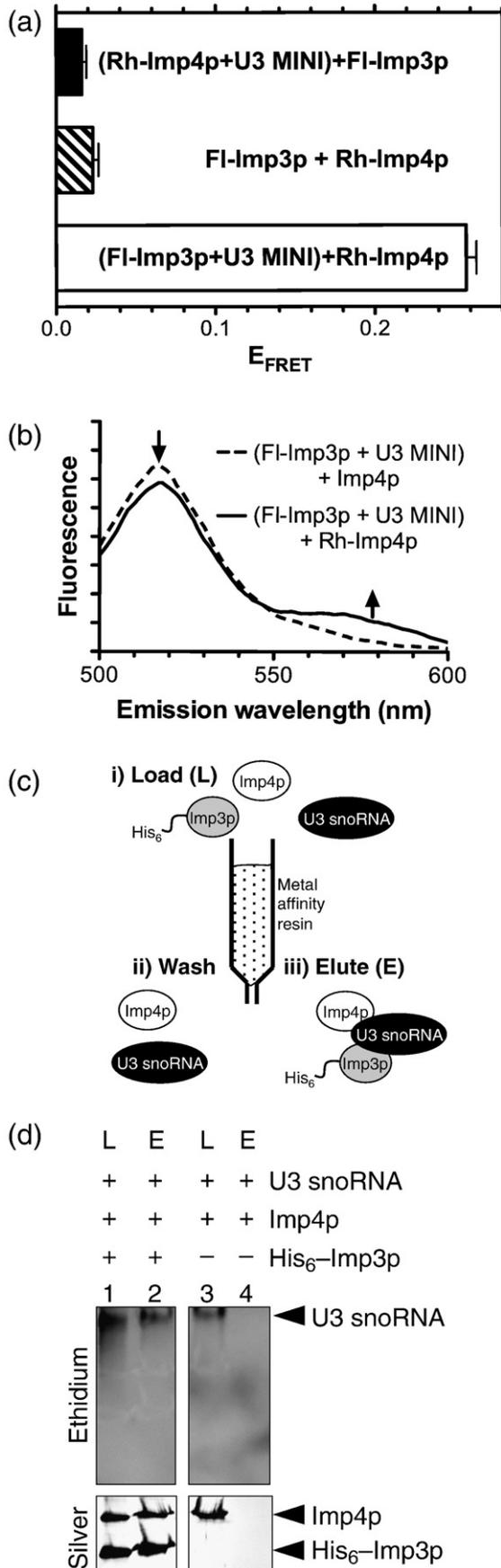
the hypothesis that Imp3p binds to U3 MINI before Imp4p.

To verify assembly of the chaperone complex with full-length U3 snoRNA, we used metal-affinity chromatography to capture N-terminal His$_6$-tagged Imp3p (His$_6$-Imp3p) in the presence of untagged Imp4p and full-length U3 snoRNA (Fig. 2c). Denaturing PAGE analysis of the loaded mixtures and eluted fractions after washes that include high salt (1 M NaCl) shows that His$_6$-Imp3p and Imp4p associate with each other in the presence of U3 snoRNA (Fig. 2d, lane 2). To confirm that retention on the column arises from interaction with the tagged protein, we showed that neither the unlabeled Imp4p nor U3 snoRNA remains bound after the washes (Fig. 2d, lane 4).

Our *in vitro* assembly findings are consistent with previous immunoprecipitation studies using *S. cerevisiae* cell extracts that showed that prior binding of Imp3p is needed to incorporate Imp4p into the SSU processome.[22] Such correlation between our *in vitro* studies and immunoprecipitation assays of others helps validate our *in vitro* system as biologically relevant.

Defining and examining a duplex formation framework

To ascertain the limits to duplex yield and hybridization rate constants, we investigated how addition of protein affects duplex stability (K_d) and duplex kinetics (k_{on} and k_{off}). Evaluation of these effects will also discriminate between the six mechanistic models that are envisioned to overcome these limitations (Fig. 3). Given that $K_d = k_{off}/k_{on}$, we determined any two of these values are sufficient to calculate the third value for a single-step model of

Fig. 2. Assembly of the chaperone complex between Imp3p, Imp4p, and U3 MINI is RNA dependent and may be ordered. (a) E_{FRET} values are shown for three conditions: addition of Fl-Imp3p to a preincubated mixture of Rh-Imp4p and U3 MINI (filled bar), a mixture of Fl-Imp3p and Rh-Imp4p (hashed bar), and addition of Rh-Imp4p to a preincubated mixture of Fl-Imp3p and U3 MINI (open bar). (b) An emission spectrum of Rh-Imp4p added to a preincubated mixture of Fl-Imp3p and U3 MINI (continuous line) illustrates the decrease in Fl emission (downward arrow) with concomitant increase in Rh emission (upward arrow) of a FRET signal. The emission spectrum of a preformed U3/Fl-Imp3p binary complex was the same in the presence (dashed line) and in the absence (data not shown) of unlabeled Imp4p, verifying that the signal is a result of FRET and not fluorescence quenching by Imp4p binding. (c) A schematic overview of the three steps of purification of the chaperone complex via metal-affinity resin: (i) His$_6$-Imp3p (gray), Imp4p (white), U3 snoRNA (black), or some combination thereof is loaded (L) onto a metal-affinity resin; (ii) the column is washed; and (iii) the eluent is eluted (E) with addition of imidazole. (d) Four L and E fractions were analyzed on SDS-PAGE stained with ethidium bromide and silver nitrate to visualize the U3 snoRNA and the proteins, respectively.
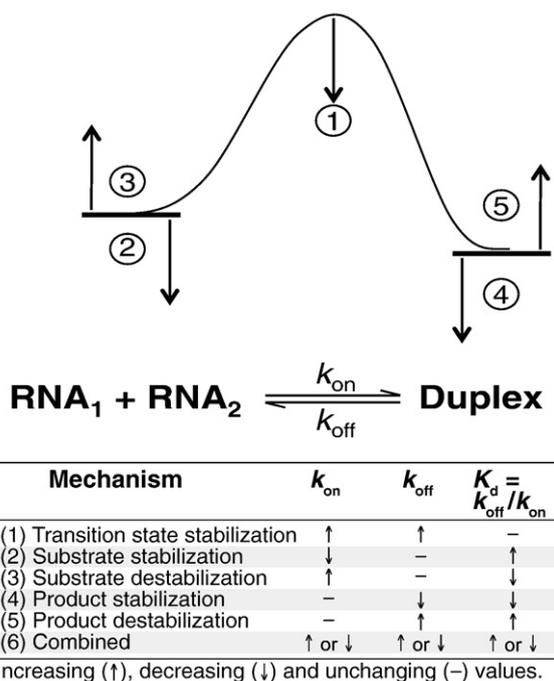
Fig. 3. Free energy reaction profiles illustrate the six possible mechanisms used by proteins to mediate duplex formation by changing the energy levels of the substrate, transition state, product, or some combination thereof. Evaluation of how the magnitude of the duplex k_{on}, k_{off}, and K_d changes after addition of protein was used to discriminate between alternate mechanisms.

reversible duplex formation as illustrated by the U3–ETS duplex (Fig. 1b). In contrast, formation of the U3–18S duplex is most readily modeled with two discernable steps: unfolding of the box A/A′ stem structure and subsequent hybridization (Fig. 1b). For the first (unfolding) step, we estimated the K_{eq} equilibrium constant between U3 MINI and its unfolded form, designated U3 MINI*, and how protein binding affects this constant. For the second (hybridization) step in U3–18S duplex formation, appropriate conditions were used to determine k_{on} (18S) and k_{off} (18S) directly rather than K_d (18S). The binding affinity is expected to include contributions from both the unfolding and hybridization steps, resulting in an apparent K_d (18S) (Fig. 1b).

Stability of the box A/A′ stem structure hinders U3–18S duplex formation

Chaperone activity can mediate U3–18S duplex formation by affecting the unfolding step, the hybridization step, or both. We begin by investigating the unfolding step (Fig. 4). To place an upper estimate on the free energy of unfolding the U3 stem structure, we obtained reversible UV melting data for U3 MINI from *S. cerevisiae* (Fig. 4a). The melting temperature of 54 °C corresponds to a free energy of 4 kcal/mol with a K_{eq} of 10^{-3} at 20 °C. As this stem structure is conserved among eukaryotes, it is expected to remain folded even at the growth tem-

perature of vertebrates (37–42 °C) with only trace quantities ($\sim 0.1\%$) of U3 MINI*, the unfolded form of U3 MINI. Helix destabilization activity is thus anticipated to ensure rapid formation of the U3–18S duplex.

Assembly of the chaperone complex opens up the U3 stem structure

To test whether assembly of the chaperone complex opens up the U3 stem structure and thereby changes K_{eq}, we used time-resolved FRET (trFRET). Unlike ssFRET, trFRET[23,24] compares the nanosecond-scale donor fluorescence decay in the presence and in the absence of the acceptor to determine with high precision the distribution of distances separating the fluorophore pair. We measured the trFRET of a doubly labeled U3 MINI with Fl at the 5′ end and Rh on the opposite side of the box A/A′ stem (Fl-U3 MINI-Rh; Fig. 4b) in the presence and in the absence of proteins and 18S (decay curves shown in Supplementary Fig. S3). Determination of the Fl–Rh distance distributions in U3 MINI alone showed that 93% of the RNA molecules yield a short (~ 19 Å) mean Fl–Rh distance (Fig. 4c, gray line), as expected from a donor and an acceptor on opposite sides of an A-form helical RNA (Fig. 4d). The remaining 7% of RNA molecules reside in a conformation of larger and more broadly distributed Fl–Rh distances (Fig. 4c, gray dashed line), consistent with the presence of a small fraction of U3 MINI dimer (Fig. 4c, inset).

Upon addition of Imp3p to Fl-U3 MINI-Rh (Fig. 4c, dashed black line), the mean Fl–Rh distance increases by 13 Å from 19 to 32 Å with a concomitant sharpening of the distance distribution (Fig. 4c, compare the continuous gray and dashed black lines). Subsequent addition of Imp4p and 18S results in only minor changes (Fig. 4c, compare the black line with the dashed and dotted black lines), supporting the view that Imp3p is primarily responsible for unfolding U3 MINI to U3 MINI*.

The 13-Å increase readily accommodates an open box A/A′ stem structure but not a fully extended U3 MINI* that could separate the Fl–Rh pair by as much as 100 Å and thus abolish FRET. To account for the lack of change in distance distributions upon addition of Imp4p and 18S, our data are most consistent with a model in which the 3′ segment of U3 MINI loops back as shown in Fig. 4d, as a result of Imp3p binding. This arrangement remains unchanged upon addition of Imp4p and 18S. Our trFRET data suggest that assembly of the chaperone complex mediates the first unfolding step by opening up the box A/A′ stem structure.

The chaperone complex accelerates U3–18S duplex formation by unfolding U3 MINI to U3 MINI*, not by stimulating k_{on} (18S)

To test whether the chaperone complex affects the second U3–18S hybridization step, we investigated

how the k_{on} (18S) and k_{off} (18S) change upon addition of Imp3p and Imp4p (Fig. 5; Table 1). In the presence of saturating amounts of protein, we determined the k_{on} (18S) by monitoring the time-dependent donor quenching of 5'-Fl-labeled U3 MINI (Fl-U3 MINI) upon addition of an equimolar amount of 3'-Rh-labeled 18S (18S-Rh). This stoichiometry was used to ensure a 1:1 donor/acceptor ratio for a maximum ssFRET signal change. Duplex formation with a k_{on} (18S) of $(7 \pm 1) \times 10^5$ M^{-1} s^{-1} was observed only after assembly of the chaperone complex (Fig. 5b, black squares, and c). To ensure that this rate directly monitors the bimolecular hybridization step, we verified that this k_{on} (18S)

was the same, within error, as that determined using more conventional pseudo-first-order conditions (excess 18S-Rh; Fig 5d).

In sharp contrast to rapid U3–18S hybridization in the presence of protein, duplex formation was not detectable in the absence of protein even when up to 1 µM concentration of 18S-Rh was used (Fig. 5b, compare the traces with open and gray circles). Likewise, no shift was detected with electrophoretic mobility shift assays using up to 200 µM U3 MINI with trace amounts of ^{32}P-labeled 18S (data not shown).

To place an upper estimate on k_{on} (18S) after the box A/A' stem has opened up, we used a fragment of U3 MINI, designated MINI-17, which retains only the 17 nucleotides involved in the U3–18S duplex, including the mismatches (the dashed box in Fig. 5a shows the MINI-17–18S duplex). The deleted flanking nucleotides of U3 MINI remove the 3' half of the box A/A' stem structure and thus eliminate the need to unfold this structure prior to U3–18S hybridization (Fig. 1b). In the absence of
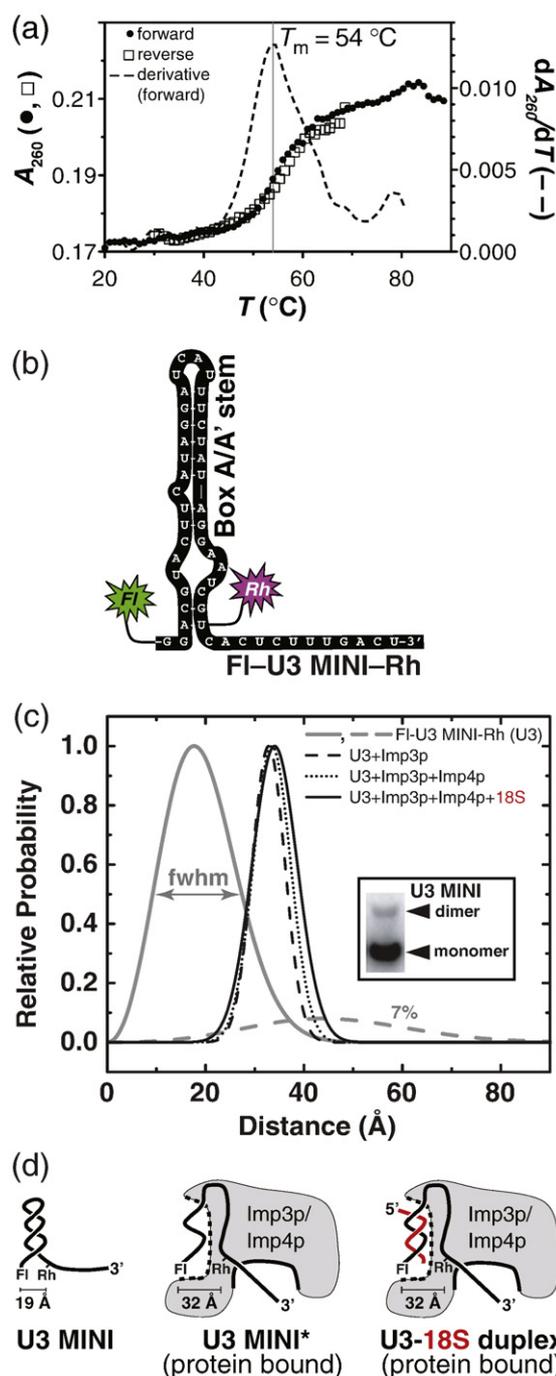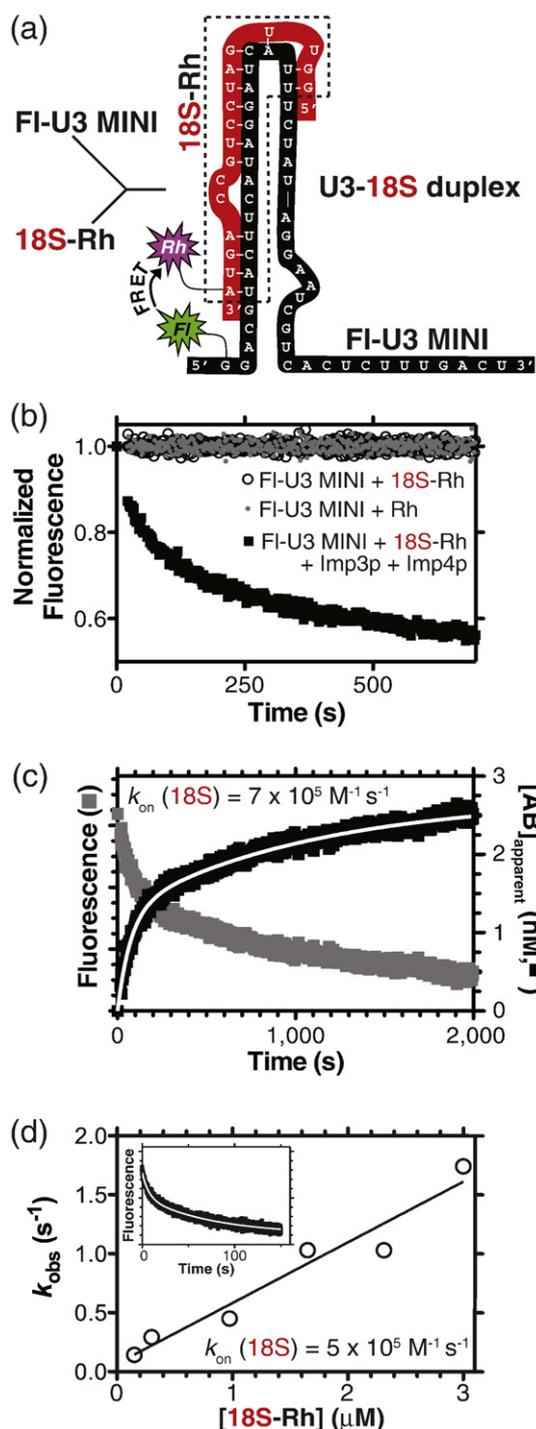
Fig. 4. The stable box A/A' stem structure of U3 MINI is unfolded to U3 MINI* by addition of protein, primarily Imp3p. (a) Optical density at 260 nm values for unlabeled U3 MINI melted in the forward direction (circles) and refolded in the reverse direction (squares). A smoothed derivative plot (dashed line) of the forward melt indicates a T_m of 54 °C, with an enthalpy of 39 kcal/mol and a $\Delta G^{\circ}_{20\ °C}$ of 4 kcal/mol. (b) trFRET was performed using a doubly labeled substrate to monitor distance changes at the base of the box A/A' stem structure: Fl is attached to the 5' end of U3 MINI via a six-carbon linker and an internal Rh label is attached via a longer succinimide linker to C5 of uracil 38. (c) FRET distance distributions between the donor and the acceptor of Fl-U3 MINI-Rh upon binding of Imp3p, Imp4p, and 18S as determined by trFRET (Supplementary Fig. S3 contains decay curves). In the absence of protein, $\sim$93% of molecules show a distance distribution centered on 19 Å (gray line), with a full width at half-maximum (fwhm) of 18 Å. The fwhm reflects in part the intrinsic flexibility of the RNA in solution. A smaller $\sim$7% (dashed gray line) has a distance distribution centered on 45 Å with an fwhm of 37 Å and is likely to result from a small population of U3 MINI dimer. With the use of an electrophoretic mobility shift assay, the inset shows that 4% $\pm$ 2% of U3 MINI exists in a dimer at the 0.5 µM concentration used for the trFRET studies. Upon binding of Imp3p (dashed black line), a single distance distribution is obtained, centered at a distance of $\sim$32 Å with an fwhm of 8 Å. Subsequent binding of Imp4p (dotted black line) and 18S (continuous black line) shows no significant additional change in distance distribution (mean distance of 33 Å with an fwhm of 9 Å and mean distance of 34 Å with an fwhm of 10 Å, respectively). (d) The simplest model indicates that the unfolded RNA nucleotides loop back to permit the separation distance to be independent of Imp4p and 18S binding. Schematics illustrate chaperone complex unfolding the box A/A' stem of U3 MINI from an A-form helix with a FRET pair separated by 19 Å (left panel) to U3 MINI*, where the separation increases to $\sim$32 Å upon binding of Imp3p and Imp4p (middle panel). Addition of 18S results in a negligible increase in the separation of the FRET pair (right panel).

protein, the k_{on} (18S) for MINI-17 hybridizing with 18S is $(7\pm1)\times10^5$ M^{-1} s^{-1} (Table 1; Supplementary Fig. S4), identical with the k_{on} (18S) observed for U3 MINI in the presence of protein (Fig. 5c). The equivalence of these rate constants supports the view that protein binding has removed the barrier to U3–18S duplex formation by unfolding the box A/A′ stem structure to expose the base-pairing site.

To determine the duplex k_{off} (18S), we chased the preformed fluorescently labeled U3–18S duplex with at least 100-fold excess of unlabeled 18S. The time-dependent exponential increase in Fl emission was

(a)

Fl-U3 MINI

18S-Rh

18S-Rh

FRET

Fl

U3-**18S** duplex

Fl-U3 MINI

5′ G G   C A C U C U U U G A C U 3′

(b)

Normalized Fluorescence

○ Fl-U3 MINI + **18S**-Rh
· Fl-U3 MINI + Rh
■ Fl-U3 MINI + **18S**-Rh + Imp3p + Imp4p

Time (s)

(c)

k_{on} (18S) = 7 × 10⁵ M⁻¹ s⁻¹

Fluorescence (■)

[AB]$_{apparent}$ (nM, ■)

Time (s)

(d)

k_{obs} (s⁻¹)

Fluorescence

Time (s)

k_{on} (18S) = 5 × 10⁵ M⁻¹ s⁻¹

[**18S**-Rh] (μM)

used to determine that k_{off} (18S) is $(2\pm1)\times10^{-3}$ s^{-1} in the presence of protein (Fig. 6a). In the absence of protein, k_{off} (18S) was not measured because formation of this duplex was not observed. To estimate k_{off} (18S) in the absence of protein, we therefore determined k_{off} (18S) for the MINI-17–18S duplex; the observed rate constant of $(1.0\pm0.1)\times10^{-4}$ s^{-1} is 20-fold slower than the U3–18S duplex dissociation rate constant in the presence of protein (Fig. 6b).

Before comparing these different substrates (U3 MINI and MINI-17), it is useful to consider the step that limits formation of other short duplexes. Classic kinetic studies have shown that hybridization of complementary nucleic acid strands proceeds via two steps: nucleation and elongation.[25] Once diffusion juxtaposes bases from two complementary strands, formation of three to four contiguous base pairs is sufficiently long-lived to nucleate the process. Elongation completes hybridization of the remaining base pairs that flank the nucleation site. Nucleation, not elongation, limits hybridization of two complementary and unstructured RNA strands to form duplexes from 8 to ~20 base pairs in length.[26] Consequently, they share the same duplex k_{on} of ~10^6 M^{-1} s^{-1}, independent of their sequence.[27,28] Equivalent k_{on} values are observed for formation of two short duplexes studied herein: the U3–18S duplex in the presence of Imp3p and Imp4p and the MINI-17–18S duplex in the absence of

Fig. 5. Hybridization kinetics of the U3–18S duplex reveal that k_{on} (18S) does not limit duplex formation. (a) The substrates used for kinetic measurements were the 5′-Fl-labeled U3 MINI (Fl-U3 MINI) and the 3′-Rh-labeled 18S (18S-Rh). The dashed box reflects the MINI-17–18S duplex (Supplementary Fig. S4). (b) Representative normalized fluorescence data are shown for ssFRET-dependent Fl quenching (10 nM Fl-U3 MINI) in the absence and in the presence of proteins upon addition of 18S-Rh (10 nM). In the absence of protein (gray circles), the trace is indistinguishable from that observed upon addition of free Rh (10 nM) (open circles) to Fl-U3 MINI, which corresponds to photobleaching. Indistinguishable traces were observed for 1 μM concentrations of substrate as well as when unlabeled 18S was added to Fl-U3 MINI in the presence or in the absence of protein (data not shown). In contrast, marked quenching is observed in the presence of saturating amounts of proteins (black squares). (c) Raw representative trace (left y-axis, gray points) is shown for Fl quenching upon addition of 18S-Rh to the Fl-U3 MINI/Imp3p/Imp4p complex to achieve a final concentration of 5 nM. The [AB]$_{apparent}$ values calculated using Eq. (1) are plotted on the right y-axis (black squares) along with the fit (white line) to Eq. (2a) to give a k_{on} (18S) of 7×10^5 M^{-1} s^{-1} (the fit was performed using molar [AB]$_{apparent}$). (d) Pseudo-first-order rates measured with a stopped-flow device are plotted for increasing concentrations of 18S-Rh ($\geq$150 nM) mixed with 38 nM Fl-U3 MINI in the presence of saturating amounts of protein. The inset shows a representative trace (150 nM 18S-Rh) of Fl quenching with k_{obs} calculated by fitting decay traces to Eq. (4). The k_{on} (18S) value determined in (c) is within the 95% confidence interval of the linear regression fit of the k_{obs} versus 18S-Rh data, which gave a k_{on} (18S) of 5×10^5 M^{-1} s^{-1}.
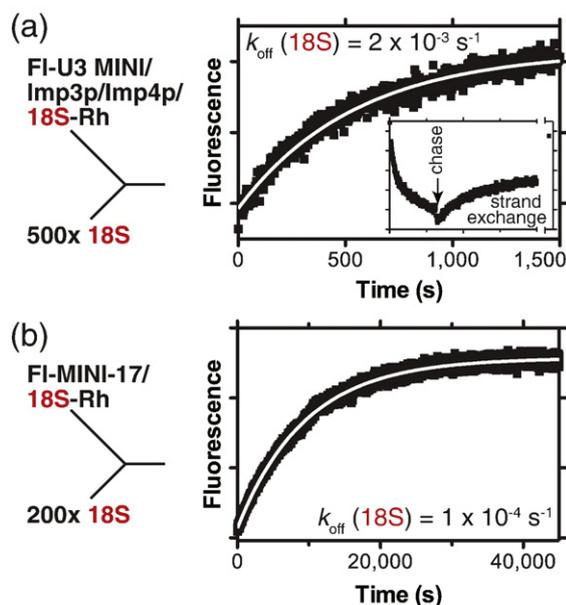
Fig. 6. Assembly of the chaperone complex increases k_{off} (18S). (a) Representative trace is shown for a chase initiated with 500-fold excess (5 μM) of unlabeled 18S to a preformed duplex between 10 nM Fl-U3 MINI and 10 nM 18S-Rh in the presence of saturating amounts of Imp3p and Imp4p. Inset shows the decrease in fluorescence due to ssFRET upon hybridization with 18S-Rh, followed by recovery of fluorescence, upon addition of unlabeled 18S, as chase is initiated. Fitting the time-dependent increase in fluorescence to Eq. (5) gave a k_{off} (18S) of 2×10^{-3} s^{-1}. (b) Representative chase trace is initiated by addition of unlabeled 18S (0.5 μM) to a preformed complex between Fl-MINI-17 (5 nM) and 18S-Rh (5 nM) in the absence of protein [k_{off} (18S) = 1×10^{-4} s^{-1}].

protein. Given the common k_{on} value, it is reasonable to expect that formation of these duplexes is also limited by nucleation.

As a result, comparing how k_{on} (18S) and k_{off} (18S) differ for the U3–18S duplex in the presence of Imp3p and Imp4p and for the MINI-17–18S duplex in the absence of protein offers insight into the mechanism of the hybridization step. Addition of Imp3p and Imp4p does not change the duplex k_{on} (18S), whereas k_{off} (18S) increases by 20-fold, corresponding to a 1.7-kcal/mol destabilization of the U3–18S duplex product [Fig. 7, compare superimposed dotted green (MINI-17–18S duplex) and black (U3–18S duplex) lines]. Of the six possible mechanisms, only product destabilization increases k_{off} (18S) and K_d (18S) without changing k_{on} (18S) (Fig. 3; Table 1). The kinetic findings provide evidence that Imp3p and Imp4p do not affect the forward hybridization barrier because k_{on} (18S) remains unchanged, but they do destabilize the product duplex after it is formed.

The findings from trFRET, UV melting, and kinetic studies suggest that protein binding accelerates formation of the U3–18S duplex by unfolding U3 MINI to U3 MINI* (the first step) instead of stimulating annealing activity (the second step). In the absence

of protein, two factors limit the amount of U3 MINI* and the subsequent U3–18S duplex (Fig. 7, gray dashed line). First, the 4 kcal/mol stability of the box A/A′ stem structure limits the percentage of U3 MINI* to 0.1% ($K_{eq} = 10^{-3}$; Fig. 4a). Second, entropy favors U3 MINI* refolding to U3 MINI rather than bimolecular hybridization. As a result, the protein-free reaction is unfavorable. In contrast, trFRET data show that U3 MINI* is the only species detected upon addition of Imp3p ($K_{eq} \gg 1$), with negligible differences observed upon subsequent addition of Imp4p and 18S (Fig. 4c and d). With an increase in K_{eq} from 10^{-3} to $\gg 1$, assembly of the chaperone complex unfolds U3 MINI into a stable U3 MINI* to accommodate annealing with 18S and ensures that the reaction proceeds energetically downhill from U3 MINI to U3 MINI* to the U3–18S duplex, in contrast to the protein-free reaction [Fig. 7, compare gray dashed (no protein) and black lines (protein added)].

Chaperone increases yield of the other hybrid: the U3–ETS duplex

Unlike the kinetic barrier that prevents detectable U3–18S duplex formation in the protein-free reaction (Fig. 5b), the yield of the other hybrid, the U3–ETS duplex, is limited by thermodynamic instability (Fig. 1b). Our previous qualitative findings showed that Imp3p and Imp4p increase the yield of the U3–ETS duplex.[16] To quantify the magnitude of this increase, we determined the K_d (ETS) and k_{on} (ETS) values by using electrophoretic mobility shift assays[16] and ssFRET assays, respectively, in the presence and in the absence of Imp3p and Imp4p (Materials and Methods). Assembly of the chaperone complex decreases the K_d (ETS) by 100-fold from $(7\pm2)\times10^{-7}$ to $(7\pm3)\times10^{-9}$ M (Fig. 8a and b; Table 2), which corresponds to an increase of 2.7 kcal/mol (20 °C) in duplex stability. We determined k_{on} (ETS) by monitoring the time-dependent donor quenching of the 3′-Fl-labeled U3 MINI (U3 MINI-Fl) upon addition of an equimolar amount of 5′-Rh-labeled ETS (Rh-ETS) in the presence and in the absence of saturating amounts of protein (Fig. 8c; Table 2). In contrast to changes in duplex affinity, k_{on} (ETS) is the same in the presence [$(5\pm1)\times10^5$ M^{-1} s^{-1}] and in the absence [$(6\pm2)\times10^5$ M^{-1} s^{-1}] of protein, within experimental error ($P>0.05$) (a representative trace of the no-protein reaction is shown in Fig. 8d). The equivalence of these k_{on} (ETS) values to the intrinsic rate constant for formation of short duplexes[27,28] supports the view that hybridization is unhindered even in the presence of Imp3p and Imp4p.

Upon assembly of the chaperone complex, the K_d (ETS) decreases by 100-fold and k_{on} (ETS) remains unchanged, favoring a product stabilization mechanism over the competing alternatives (Fig. 3). A change in K_d rules out transition-state stabilization, whereas no change to k_{on} rules out substrate stabilization and destabilization, as well as a
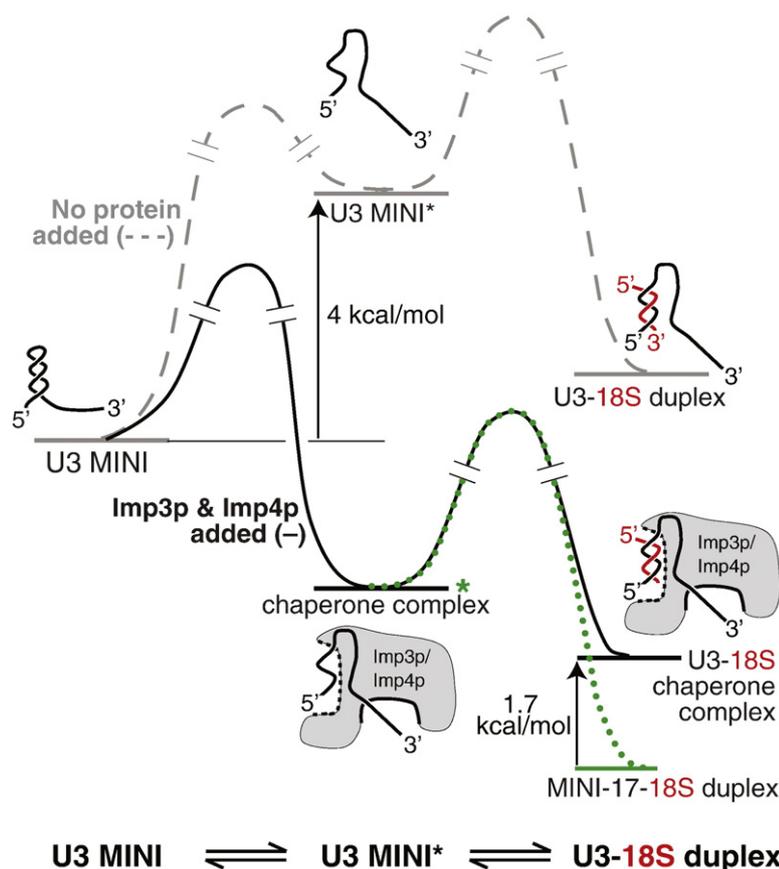
Fig. 7. Reaction profiles illustrating a model for how protein binding accelerates U3–18S duplex formation by unfolding U3 MINI to U3 MINI* (the first step) rather than stimulating hybridization (the second step). In the absence of protein (dashed gray line), the 4 kcal/mol needed to unfold U3 MINI (Fig. 4a) limits the quantities of U3 MINI* and thus reduces the subsequent product duplex to an undetectable level. In contrast, protein binding (black line) unfolds U3 MINI to form a stable U3 MINI* (Fig. 4c), thereby allowing the hybridization step to occur at the intrinsic rate constant for hybridizing short duplexes ($\sim 10^6$ M^{-1} s^{-1}) with energetically favorable transitions from U3 MINI to U3 MINI* to duplex. Because hybridization of the MINI-17–18S duplex in the absence of protein (green dotted line) and that of the U3–18S duplex in the presence of protein (black line) share a common rate-limiting step, comparison of these reactions is useful. Superimposing the energy of MINI-17 (asterisk) and that of the chaperone complex shows the same barrier for the forward reaction [identical k_{on} (18S) values]; however, a 20-fold increase in k_{off} (18S) by the chaperone complex results in 1.7 kcal/mol of product destabilization (Table 1). The energy levels thus differ for the protein-bound U3–18S duplex and the protein-free MINI-17–18S duplex.

combined mechanism. By multiplying K_d (ETS) and k_{on} (ETS), k_{off} (ETS) is predicted to increase, which rules out product destabilization. Product stabilization is the only model in which protein decreases K_d without changing k_{on}. The absence of a change to k_{on} (ETS) upon addition of protein reflects an unchanged hybridization barrier (Fig. 9). After hybridization, the protein stabilizes this duplex by 2.7 kcal/mol to ensure high yield.
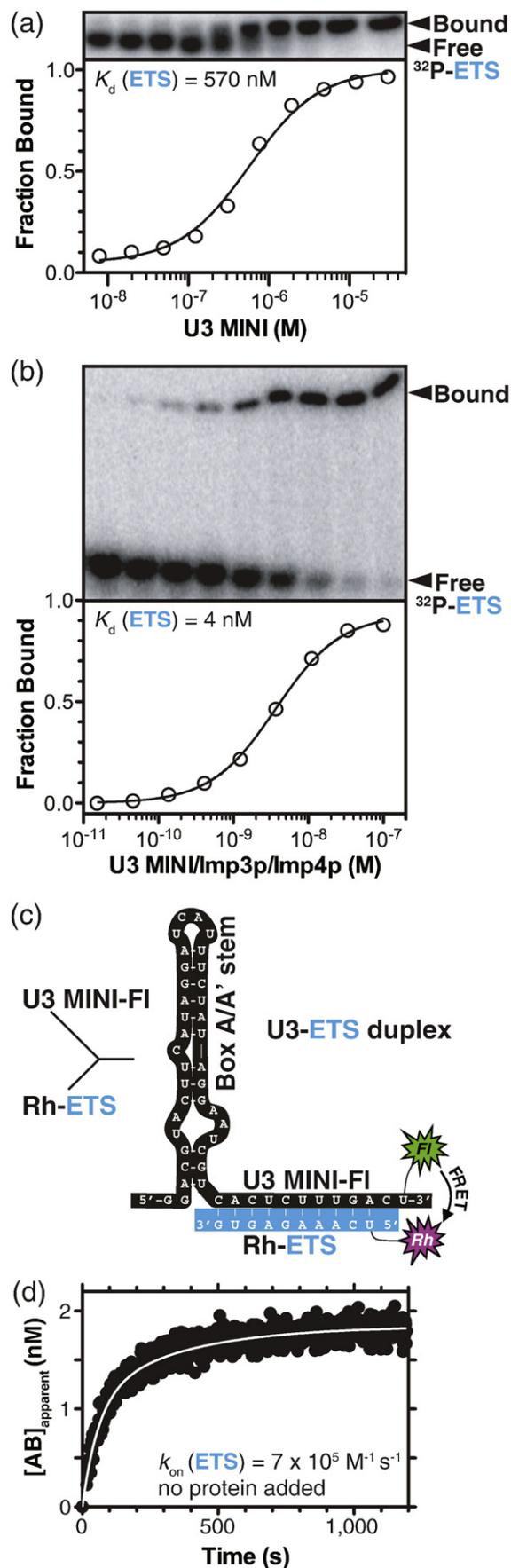
Our findings support a model in which the U3–ETS duplex product is stabilized by docking into a binding pocket created by Imp3p and Imp4p (Fig. 9). Duplex docking is expected to occur only after the duplex forms because the k_{on} (ETS) is unaffected by the presence of protein (Table 2) and the U3 nucleotides involved in hybridization are accessible to ribonuclease digestion.[16] A concave binding pocket is an attractive possibility because it most readily accommodates the cylindrical shape of the A-form duplex product.

Chaperone sufficiently enhances formation and yield of both duplexes

By extrapolating our findings using minimal substrates *in vitro* to the corresponding reactions occurring with full-length pre-rRNA and U3 snoRNA, we can estimate whether the chaperone complex satisfies the *in vivo* demands for rapid formation and high yield of the U3–pre-rRNA duplexes. Addition of the extra pre-rRNA sequences and the numerous *trans*-acting factors found *in vivo* will undoubtedly affect these results. However, given the many potential complications arising from misfolding of larger RNA substrates, it is important to first determine how RNA chaperones alter duplex formation rates and the yields of minimal RNA substrates.

The nucleolar concentrations of U3 snoRNA and the pre-rRNA are required to calculate duplex rates and yields that simulate *in vivo* conditions. Even though these values are unknown, estimates are possible. High-resolution mapping of rDNA and U3 snoRNA territories in the nucleolus of *S. cerevisiae* using optical microscopy indicates volumes of 0.5×10^{-15} and 1.5×10^{-15} L, respectively.[29] Given that about 4000 copies of pre-rRNA[30] and between 400 and 1000 copies of U3 snoRNA[31] are expected for rapidly growing cells, the concentration of the U3 snoRNA is between 0.4 and 1 μM and that of the pre-rRNA is $\sim$13 μM. Undoubtedly, the concentration will not be homogeneous throughout the nucleolus; hence, our calculations use a broad concentration range from 0.01 to 10 μM. It is also possible to approximate the yield of the U3–pre-rRNA duplexes *in vivo*. About 1 in 10 pre-rRNA transcripts is cleaved at A_3 before A_2 (and A_0 and A_1; Fig. 1a), resulting in a 23S intermediate rather than the standard 20S precursor [K. Karbstein (University of Michigan),

Fig. 8. Chaperone complex stabilizes the U3–ETS duplex without affecting the association rate constant [k_{on} (ETS)]. Representative binding data from electrophoretic mobility shift assays for ^{32}P-labeled ETS-U3 MINI duplex in the absence (a) and in the presence (b) of the chaperone complex. Fraction bound is calculated based on the fraction of ^{32}P-labeled ETS shifted and plotted against increasing concentration of either U3 MINI or the chaperone complex. K_d (ETS) is calculated by fitting the fraction bound to Eq. (6). (c) The fluorescently labeled U3–ETS duplex substrate used for kinetic assays includes the donor 3′-Fl-labeled U3 MINI (U3 MINI-Fl) and the acceptor 5′-Rh-labeled ETS (Rh-ETS). (d) Representative trace for measurement of k_{on} (ETS) for 5 nM U3 MINI-Fl and 5 nM Rh-ETS in the absence of protein. The fractional change in ssFRET-dependent donor quenching is proportional to [AB]$_{apparent}$ in Eq. (1); k_{on} (ETS) is calculated using Eq. (2a) (the fit was performed using molar [AB]$_{apparent}$).

personal communication]. Because U3–pre-rRNA hybridization is a prerequisite for the A_0–A_2 cleavages, it is reasonable to assume that these duplexes have not yet formed in the 23S intermediates. Given these considerations, we estimate that 90% of the pre-rRNA forms a duplex with the U3 snoRNA *in vivo*.

To assess whether the chaperone complex sufficiently accelerates the rate of U3–18S duplex formation, we calculated half-lives for the reaction as a function of substrate concentration (Fig. 10a is based on values in Table 1). As described in Introduction, formation of the U3–18S duplex is a prerequisite for the U3-dependent cleavages that release the 18S precursor from the pre-rRNA. In rapidly growing cells, these cleavage events have an estimated half-life of 85 s *in vivo*.[15] The prerequisite formation of the U3–18S duplex is thus expected to be even faster. In the absence of Imp3p and Imp4p, the formation of the U3–18S duplex is not observed. In sharp contrast, in the presence of protein, the half-life for duplex formation is less than 85 s when the pre-rRNA concentration exceeds 7 nM (based on the kinetic parameters in Table 1). This analysis supports the argument that Imp3p and Imp4p are necessary and sufficient to fulfill the need for rapid formation of this duplex *in vivo*.

Consistent with *in vivo* expectations, the presence of Imp3p and Imp4p ensures a high U3–ETS duplex yield over a broad concentration range of both substrates (U3 snoRNA and pre-rRNA) based on calculated percentage yield (Fig. 10b and c). In the absence of protein, pre-rRNA and U3 snoRNA (assuming equimolar amounts) must exceed estimates of their nucleolar concentrations (>63 μM) to achieve high duplex yield (>90%). In contrast, lower substrate concentrations (>0.63 μM), in line with *in vivo* estimates, are sufficient to ensure high U3–ETS duplex yield in the presence of Imp3p and Imp4p.

The U3–ETS and U3–18S hybridizations were modeled as separate bimolecular reactions because the pre-rRNA was divided into two minimal substrates (ETS and 18S); however, intramolecular reactions may also occur *in vivo* with full-length pre-rRNA (Fig. 1a). During pre-rRNA transcription, the

Table 2. U3–ETS duplex kinetic and thermodynamic parameters

	No protein added	Imp3p and Imp4p added	Fold change	$\Delta\Delta G$ (kcal/mol)
K_d (ETS)	$(7\pm2)\times10^{-7}$ M	$(7\pm3)\times10^{-9}$ M	~100-fold decrease	-2.7[a]
k_{on} (ETS)	$(6\pm2)\times10^{5}$ M^{-1} s^{-1}	$(5\pm1)\times10^{5}$ M^{-1} s^{-1}	Not significant[b]	~0
k_{off} (ETS)[c]	0.42 s^{-1}	3.5×10^{-3} s^{-1}		

[a] $\Delta\Delta G = -RT[ln(K_{d\ (no\ protein\ added)}/K_{d\ (protein\ added)})]$ at 20 °C.
[b] $P > 0.05$.
[c] Calculated from k_{on} (ETS) and K_d (ETS) values.

U3–ETS duplex may hybridize first as a bimolecular reaction because the ETS site is transcribed before the 18S site. A stable U3–ETS duplex is needed for subsequent intramolecular U3–18S hybridization. The half-life for this intramolecular reaction may occur even faster than those in Fig. 10a due to higher effective concentration (lower entropic barrier). It is reasonable to assume that unfolding of the box A/A′ stem structure will still limit the U3–18S reaction in the absence of protein. Our *in vitro* studies provide evidence that the presence of Imp3p and Imp4p will alleviate this kinetic unfolding barrier to accelerate U3–18S hybridization and enhance the stability of the U3–ETS duplex.

Discussion

In ribosome biogenesis, the U3/Imp3p/Imp4p chaperone complex is expected to position the SSU processome for the early pre-rRNA cleavage events that release the SSU precursor by stimulating docking between the U3 snoRNA and two complementary sites on the pre-rRNA: the U3–ETS and U3–18S duplexes (Fig. 1). Formation of these duplexes has to be fast[15] (estimated half-life <85 s) and efficient[6–11] (estimated duplex yield >90%) to keep up with the high demand that rapidly growing cells have for producing ribosomes. In this study, we developed *in vitro* ssFRET- and trFRET-based assays to demonstrate assembly of the chaperone complex (Fig. 2) and show that it possesses the RNA chaperone activities

(Figs. 4–6 and 8) necessary to satisfy these *in vivo* demands (Fig. 10).

The chaperone complex sufficiently stimulates U3–18S duplex formation

In the absence of protein, formation of the U3–18S duplex is not observed *in vitro* but is expected to occur in two steps: unfolding of U3 MINI to U3 MINI* and hybridization (Figs. 1b and 7). Assembly of the chaperone complex, and particularly binding of Imp3p, destabilizes the conserved box A/A′ stem structure to expose its 18S base-pairing site by unfolding U3 MINI to U3 MINI* (Figs. 1b and 4). Unfolding this stem structure is sufficient to accelerate this reaction from an undetectable rate to the intrinsic hybridization rate for short duplexes (~10^6 M^{-1} s^{-1}).

The U3–18S chaperone activity is expected to be needed throughout the eukaryotic kingdom of life because the box A/A′ structure, the pre-rRNA base-pairing potential,[18–20] and the sequences of Imp3p and Imp4p are conserved.[17,21] In the absence of protein, formation of the U3–18S duplex is not observed. In contrast, in the presence of Imp3p and Imp4p, rapid formation of this duplex occurs over a wide range of substrate concentrations (Fig. 10a).

The chaperone complex ensures sufficiently high U3–ETS duplex yield

The chaperone complex stabilizes the duplex by decreasing the K_d (ETS) by ~100-fold (Figs. 8–10;

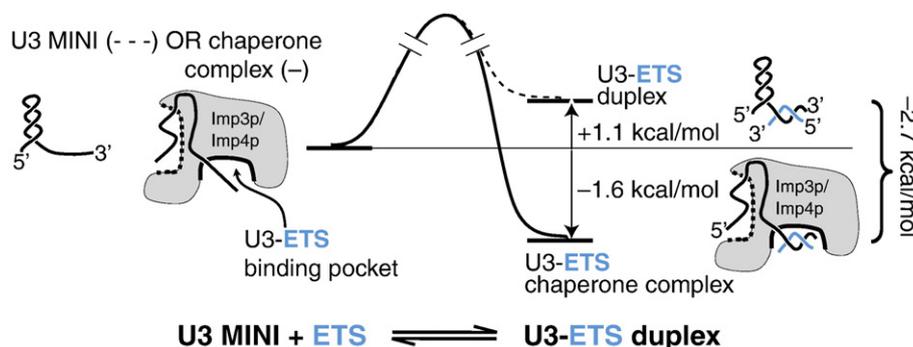**U3 MINI + ETS ⇌ U3-ETS duplex**

Fig. 9. Reaction profile illustrating a product stabilization model for the U3–ETS duplex mediated by Imp3p and Imp4p in the chaperone complex. The reaction proceeds from U3 MINI (on the left) to the U3–ETS duplex (on the right) with the same barrier height because k_{on} values remain unchanged in the absence (dashed line) and in the presence (continuous line) of Imp3p and Imp4p. In the proposed product, stabilization mechanism formation of the U3–ETS duplex occurs spontaneously. Once formed, the duplex binds tightly into a pocket created by Imp3p and Imp4p to increase duplex stability. The free energy difference between the reactants (free RNAs) and the U3–ETS duplexes in the presence and in the absence of the chaperone complex assumed a standard state of 100 nM and 20 °C and used the K_d (ETS) values from Table 2.
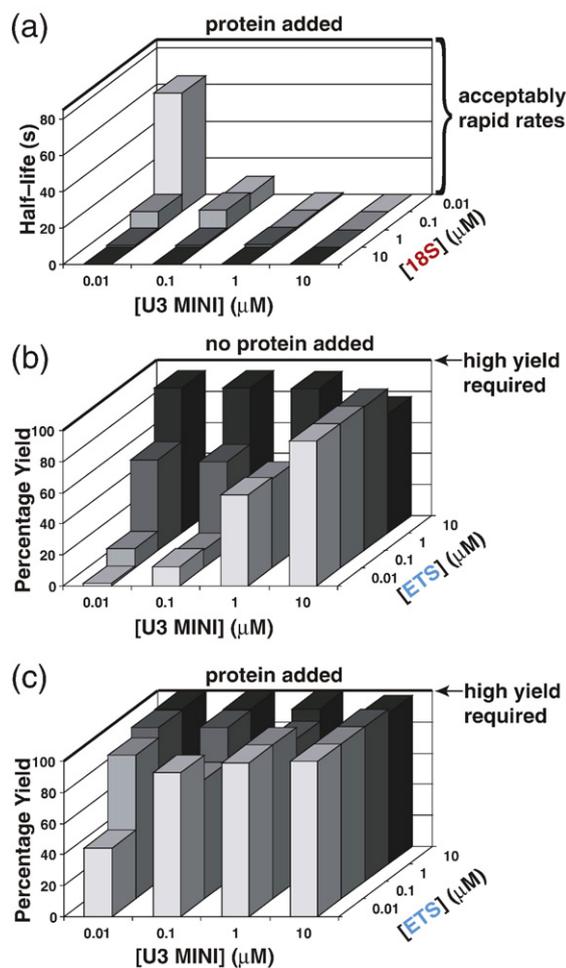
Fig. 10. The chaperone complex ensures rapid hybridization and a high duplex yield for the U3–pre-rRNA duplexes. (a) U3–18S hybridization is a prerequisite for cleavage and release of pre-r18S, which has a half-life of 85 s *in vivo*.[15] In the presence of proteins, the half-life for hybridization is faster than 85 s, for all concentrations greater than 7 nM, thus satisfying cellular requirements, calculated using Eq. (3) and values from Table 1. (b) The percentage yield of the U3–ETS duplex [using Eq. (7) and values from Table 2] in the absence of protein is below 90% for substrate concentrations less than 63 μM. (c) In the presence of protein, yield increases to 90%–100% for substrate concentrations greater than 630 nM. High U3–pre-rRNA yield is required for rapidly growing yeast cells and is observed only in the presence of the chaperone complex.

Table 2) to ensure high yield of the U3–ETS duplex over a physiologically relevant range of pre-rRNA concentrations. The chaperone complex binds to the U3–ETS duplex after it is formed to increase the duplex stability by 2.7 kcal/mol. Even though high nucleolar concentrations of pre-rRNA and U3 snoRNA are expected, the chaperone complex is needed to ensure high duplex yield when the concentration of both substrates is less than 630 nM (with equimolar substrate concentrations).

Product stabilization of the U3–ETS duplex may be needed throughout the eukaryotic kingdom. Previous studies of the chaperone activities of Imp3p and Imp4p indicate that they are not very sensitive to sequence variation of the U3–ETS duplex as long as hybridization potential is maintained.[9,16] Thus, in single-cell eukaryotes, where short U3–ETS base pairing is conserved, the chaperone complex ensures that high U3–ETS duplex yield limits neither ribosome biogenesis nor rapid cell growth. In the frog *Xenopus laevis* and other higher eukaryotes, the one short U3–ETS duplex is replaced by two short duplexes separated by a number of nucleotides.[32] More study is needed to establish whether a chaperone complex stabilizes one or both of these duplexes, which are expected to be unstable due to their short lengths.

Implications for ribosome biogenesis

With quantitative data on hand, it is possible to estimate the need for *trans*-acting factors to release the SSU precursor from the SSU processome (U3–18S dissociation) or to recycle the SSU processome for another round of pre-rRNA processing (U3–ETS dissociation) (Fig. 1). Earlier qualitative analysis showed that removal of Imp3p and Imp4p from the U3–ETS duplex leads to duplex dissociation.[16] To estimate the need for "release factors" for dissociation of the ETS portion of the pre-rRNA, we calculated k_{off} (ETS) values and corresponding dissociation half-lives (Table 2). Addition of Imp3p and Imp4p increases the dissociation half-lives from ∼2 to ∼200 s. Given the ∼85 s half-life for the U3-dependent cleavages, protein is required to ensure that the U3–ETS duplexes remain intact long enough for cleavage to occur. For release of the 18S portion of the pre-rRNA, dissociation half-lives were calculated from observed k_{off} (18S) values (Table 1). Addition of Imp3p and Imp4p decreases the dissociation half-life from ∼2 h to ∼350 s. Protein addition thus reduces the need for helicase activity while ensuring that the U3–18S duplex remains intact long enough to release the SSU precursor. Possibly, proteins are used to temporally regulate the U3–18S duplex dissociation that releases the 18S nucleotides, which are part of a universal pseudoknot structure of mature ribosomes.[10] Releasing these 18S nucleotides at the proper time chaperones 18S folding by ensuring that this centrally located pseudoknot does not form prematurely and that these nucleotides are not trapped in an incorrect structure.

Reducing chaperone activity toward incorrect targets

Proteins and RNA chaperones often do not possess specific activity; rather, they target a large number of substrates. Protein chaperones preferentially bind to misfolded proteins by recognizing exposed hydrophobic patches that serve as distinctive features to avoid targeting correctly folded substrates, which may be harmful. How RNA chaperones avoid this problem is less clear because misfolded and correctly folded RNAs offer few if any distinguishing recognition features. A recent study by Bhaskaran and

Russell[33] showed that for one substrate the increased stability of the correctly folded RNA compared with its misfolded counterpart protects it from the unwanted attention of RNA chaperones. Our studies illustrate another strategy whereby the RNA chaperone acts site specifically. Imp3p and Imp4p preferentially bind to the 5′ portion of the U3 snoRNA,[16] and because assembly is RNA dependent (Fig. 2), the chaperone complex targets a specific site.

Conclusions

Our kinetic and thermodynamic framework predicts that the chaperone complex is needed to accelerate U3–18S duplex formation from an undetectable rate to $\sim 10^6 \, M^{-1} \, s^{-1}$ and thereby ensure that this process limits neither ribosome biogenesis nor rapid cell growth. In contrast, the 2.7 kcal/mol of U3–ETS duplex stabilization provided by the chaperone complex will help, but may not be essential, in achieving the needed high duplex yield given the high concentrations of U3 snoRNA and pre-rRNA expected in the nucleolus. Determining how proteins change the k_{on}, k_{off}, and K_d of RNA duplexes is a general strategy to investigate the mechanism by which other RNA chaperones satisfy the cellular demands for fast, efficient, and site-specific structural rearrangements.

Materials and Methods

Details of the trFRET assays and derivation of equations for determining k_{on} under non-pseudo-first-order conditions are found in Supplementary Materials and Methods.

Assembly of complexes and overview of assays

All reactions were carried out in reaction buffer (20 mM Tris, pH 8.0, 100 mM KCl, 30 mM NH$_4$Cl, and 0.5 mM MgCl$_2$) at 20 °C unless otherwise specified. Prior to use, U3 MINI was refolded in a manner to maximize formation of the box A/A′ stem relative to dimer formation: samples were heated to >90 °C for 2 min and then incubated for 10 min on ice. The chaperone complex was assembled by incubating heat-annealed U3 MINI with saturating amounts of Imp3p ($\geq 1.5 \, \mu M$) for 60 min. Subsequently, Imp4p was added at saturating amounts ($\geq 0.5 \, \mu M$) and allowed to reach equilibrium for at least 30 min.

In FRET-based assays, we used Fl as the donor (excitation peak at 493 nm and emission peak at 520 nm) and Rh as the acceptor (excitation peak at 550 nm and emission peak at 580 nm). E_{FRET} values were calculated as described before[34] by determining the Fl and Rh emission peak heights and correcting them for direct acceptor excitation.

Protein purification and labeling

Imp3p and Imp4p from *S. cerevisiae* were recombinantly expressed and purified as described before.[16] Imp3p and Imp4p were labeled with Fl and Rh. Fl-5-maleimide was reacted with Imp3p to make Fl-Imp3p by forming thioether linkages with cysteine residues according to the recommendations of the manufacturer (Invitrogen). Like-wise, Rh-5-maleimide was reacted with Imp4p to make Rh-Imp4p.

The pHis$_6$-Imp3p expression vector contained the Imp3 open-reading frame, and the N-terminal MGSSHHHHH-HSSGLVPRGSH tag was cloned into pET21d using XbaI and NotI restriction sites (New England Biolabs). His$_6$-Imp3p was expressed at 16 °C overnight (16–17 h) in *Escherichia coli* BL21(DE3) cells supplemented with a vector coding for rare tRNA^{Arg} codons as described before.[35] After cell breakage in 20 mM Tris, pH 8.0, and 200 mM NaCl, inclusion bodies were solubilized in 20 mM Tris, pH 8.0, 600 mM NH$_4$Cl, 50 mM Mes (4-morpholine-ethanesulfonic acid), pH 6.5, and 1 M urea. The solubilized protein was purified via Talon resin (Clontech) by following the recommendations of the manufacturer and stored at a concentration of $\geq 70 \, \mu M$ in 20 mM Tris, pH 8.0, and 50 mM MgCl$_2$.

RNA synthesis and labeling

All modified RNA molecules represent *S. cerevisiae* sequences and were synthesized and PAGE purified by Dharmacon to ensure complete label incorporation. Both fluorophores must be freely rotating to ensure that E_{FRET} values reflect the distance between the donor and the acceptor. To enable this mobility, we attached each fluorophore via a six-carbon linker to its RNA oligomer and verified that the fluorescence polarization values were <0.3. To label with Rh, RNA oligomers were synthesized with an amino group at the 3′ terminus, 5′ terminus or internally at C5 of one uracil residue and then reacted with Rh-succinimide (5-TAMRA, Invitrogen) according to the recommendations of the manufacturer. 5′-Fl was attached during synthesis. To label with Fl at the 3′ terminus, RNA oligomers were synthesized with an amino group and then reacted with Fl-succinimide (6-FAM, Invitrogen) according to the recommendations of the manufacturer.

U3 MINI (5′-GGA CGU ACU UCA UAG GAU CAU UUC UAU AGG AAU CGU CAC UCU UUG ACU) represents nucleotides 4–50 of the U3 snoRNA with an additional 5′-terminal G, added originally to enable T7 *in vitro* transcription.[16] MINI-17 (5′-UAC UUC AUA GGA UCA UU) includes only the U3 nucleotides involved in 18S hybridization (the dashed box in Fig. 5a represents the MINI-17–18S duplex). The ETS site 5′-UCA AAG AGU G reflects nucleotides 470–479 of the pre-rRNA, and the 18S site 5′-GGU UGA UCC UGC CAG UA reflects nucleotides 6–22 of the mature 18S rRNA.

Metal-affinity chromatography

The chaperone complex was made using His$_6$-Imp3p, Imp4p, and U3 snoRNA in a 50 μL volume, and complexes were separated via metal-affinity chromatography. The U3 snoRNA was produced by run-off transcription using a linearized plasmid DNA template.[16] The template was digested with DNase I (Promega), and nucleotides less than ~ 200 nucleotides, including abortive transcripts, were removed with the use of an RNeasy MINI Kit (Qiagen). Before use, the U3 snoRNA was refolded: the RNA was incubated at 100 °C (3 min), cooled at room temperature (3 min), and then incubated with 10 mM MgCl$_2$ at 55 °C (3 min). Prior to loading, 50 μL Co^{2+} Talon affinity resin (Clontech) was preequilibrated with 10 column volumes of reaction buffer. Protein and RNA complexes containing His$_6$-Imp3p bound to the metal-affinity resin, whereas excess untagged RNA and protein

were eluted with a series of washes: 5 column volumes of reaction buffer, 2 column volumes of reaction buffer with increased ionic strength (1 M NaCl added), and 3 column volumes of reaction buffer to restore the ionic strength of the column. The 1 M salt wash was necessary to eliminate nonspecific Imp4p–resin interaction. Complexes captured by the affinity resin were eluted with 4 column volumes of 300 mM imidazole in reaction buffer and resolved on 15% denaturing SDS-PAGE. Protein and RNA molecules were visualized by silver staining and ethidium bromide, respectively.

UV melts

UV absorbance melting curves were collected at 260 nm from 10.5 to 84.5 °C in 1-deg increments on a Varian Cary 1E UV-Visible Spectrophotometer using unlabeled U3 MINI in reaction buffer. The absorption and temperature were processed using the program PRISM. The slope at the midpoint of the transition in a plot of normalized A_{260} *versus* T (K) was used to estimate ΔH (at T_m) and $\Delta G°$ (at 20 °C) as previously described for a single transition.[36]

Hybridization assays and half-life ($t_{1/2}$) for the U3–18S duplex

To monitor U3–18S duplex association rates, we used two methods. Stopped-flow kinetics were used to measure k_{on} (18S) under pseudo-first-order conditions where [18S-Rh] greatly exceeds [Fl-U3 MINI] throughout the titration. Rapid-mixing techniques were used to measure k_{on} (18S) under non-pseudo-first-order conditions where [18S-Rh] equals [Fl-U3 MINI]. The latter condition ensures a 1:1 donor/acceptor ratio for a maximum ssFRET signal change. In the presence of protein, 2, 5, 10, and 15 nM equimolar substrate concentrations were used. No reaction was detected in the absence of protein. For assays monitoring MINI-17–18S duplex formation 2, 5, and 10 nM equimolar substrate concentrations were used.

An SLM 8000C Spectrofluorimeter was used to collect data under non-pseudo-first-order conditions in which the concentrations of the FRET donor and acceptor were equal. Excitation and emission slits were set to 2 and 4 mm, respectively. Integration time was set at 1 s, and emission counts were recorded as a function of time to provide an optimal signal of at least 4000 counts. The fractional decrease in the fluorescence of Fl-U3 MINI is proportional to the fractional increase in the amount of U3–18S duplex ([AB]$_{apparent}$, M) formed and thus can be calculated using:

$$[AB]_{apparent} = \left[1 - \frac{f_t}{f_0}\right] A_0 \tag{1}$$

where f_0 is the fluorescence at time $t = 0$, f_t is the fluorescence at any time t, and A_0 is the concentration of limiting substrate, either Fl-U3 MINI or 18S-Rh. In this case, since Fl-U3 MINI and 18S-Rh are equimolar, A_0 can be either one. The rate of duplex hybridization is similar to a bimolecular reversible reaction, which under equimolar concentrations has a form of the first term in Eq. (2a) below (see Supplementary Materials and Methods for derivation of Eq. (2a–e)):

$$[AB]_{apparent} = x_{eq} \frac{1 - e^{-zt}}{1 + we^{-zt}} + d\left(1 - e^{-k_{pb}t}\right) \tag{2a}$$

where

$$b = -2k_{on}A_0 - k_{off} \tag{2b}$$

$$z = \sqrt{b^2 - 4k_{on}^2 A_0^2} \tag{2c}$$

$$w = \frac{-(b + z)}{(b - z)} \tag{2d}$$

$$x_{eq} = -\frac{(b + z)}{2k_{on}} \tag{2e}$$

A second exponential parameter with k_{pb} as the rate constant and d as the amplitude is added to Supplementary Eq. (S9) to account for photobleaching. The region of the data that defines k_{off} (18S) overlaps the contribution from photobleaching and thus limits the ability to calculate k_{off} (18S) from these data.

To determine the half-life $t_{1/2}$ for the U3–18S duplex, we set $\frac{x}{x_{eq}}$ to 0.5 and solved for t:

$$t_{1/2} = \frac{1}{z} \ln\left(2 - \frac{b + z}{b - z}\right) \tag{3}$$

Hybridization rate constants were also determined for substrates labeled at different sites to verify that the fluorophores did not bias our measurements: unlabeled U3 MINI and doubly labeled 18S (Fl-18S-Rh). Reactions were initiated by adding a preformed ternary complex to Fl-18S-Rh.

For pseudo-first-order conditions, increasing concentrations of 18S-Rh (150 to 3000 nM) were mixed in a stopped-flow reactor (SLM Aminco FP-120) with a preformed ternary complex with a final concentration of 38 nM Fl-U3 MINI and saturating amounts of Imp3p and Imp4p. FRET-dependent Fl quenching was recorded with minimum 1-ms resolution at 520 nm as a function of time with an AB2 Luminescence Spectrophotometer version 5.31 using a slit width of 2 nm for excitation (at 490 nm) and that of 16 nm for emission (at 520 nm). Data were averaged for a minimum of eight shots per concentration of 18S-Rh. A representative averaged decay trace for 150 nM 18S-Rh is shown in the inset of Fig. 5d. The rate constant k_{obs} was calculated by fitting decay traces to:

$$f = A + Be^{-k_{obs}t} + Ce^{-k_{obs2}t} \tag{4}$$

where f is the fluorescence, A is f at infinite time, and B and C reflect the amplitude of each exponential with rate constants k_{obs} and k_{obs2}, respectively. The fast phase (k_{obs}) increased with increasing concentrations of 18S-Rh. The slow phase (k_{obs2}) has a rate consistent with that of the photobleaching from the fluorophore and shows negligible dependence on concentration of 18S-Rh and was thus assigned k_{obs2} as the photobleaching rate constant.

Determination of the U3–18S duplex dissociation rate constant [k_{off} (18S)]

The k_{off} (18S) was determined by chasing a preformed duplex of Fl-U3 MINI and 18S-Rh with a large excess of unlabeled 18S (>100-fold) in the presence of saturating amounts of protein. The chase resulted in an exponential growth of the Fl emission as RNA molecules with no FRET signal (Fl-U3 MINI–18S duplex and liberated 18S-Rh)

replaced those with a FRET signal (Fl-U3 MINI–18S-Rh duplex). To determine k_{off} (18S), we fit the time-dependent increase in the Fl fluorescence to:

$$f = f_{max}\left(1 - e^{-k_{off}t}\right) + f_0 \qquad (5)$$

where f is the fluorescence at any time t, f_0 is the fluorescence before chase is initiated, and $f_{max} + f_0$ is f at infinite time. The rate constant k_{off} (18S) is determined under conditions where [18S] is high enough to ensure that this rate constant is independent of [18S]. The same method was used to determine k_{off} (18S) for Fl-MINI-17 and 18S-Rh.

Binding affinities [K_d (ETS)] and percentage yield for the U3–ETS duplex

To determine K_d (ETS) values for the U3–pre-rRNA duplexes, we titrated U3 MINI with trace amounts of ^{32}P-5′-end-labeled ETS either in the presence or in the absence of saturating amounts of Imp3p and Imp4p in reaction buffer. The RNA complexes were allowed to incubate for ~45 min and were resolved on 12% (absence of proteins) and 6% (presence of proteins) nondenaturing PAGE gel (50:1 cross-linking ratio) for 45 min at 125 V at 4 °C. The gel was polymerized with 40 mM Tris-acetate, pH 8.0, 1 mM ethylenediaminetetraacetic acid, 50 mM KCl, and 2.5% (v/v) glycerol, and the same was used as the running buffer. An equal volume of 40% (w/v) sucrose, 50 mM KCl, and 80 mM Tris-acetate, pH 8.0, was added to the samples just before loading to allow the sample to sink in the well. The bound and free ^{32}P-labeled ETS species were visualized by autoradiography using a Fuji imaging plate (Bas 2024) and Typhoon 9400 (Amersham Biosciences, GE) and quantified using Image Quant 5.0. K_d values were determined by fitting the fraction of ^{32}P-labeled ETS bound as a function of [U3 MINI] in the absence or in the presence of protein using:

$$\text{Fraction Bound} = \frac{Y_{max}[\text{U3 MINI}]}{K_d + [\text{U3 MINI}]} + Y_{min} \qquad (6)$$

where Y_{max} and Y_{min} are the fraction-bound values at saturating and limiting [U3 MINI], respectively.

The quadratic solution to binding equations was used to calculate the duplex yield from K_d (ETS) values using:

Percentage Yield

$$= \left[\frac{(K_d + A + B) - \sqrt{(K_d + A + B)^2 - (4AB)}}{2 \times \min(A,B)}\right] \times 100 \qquad (7)$$

where K_d is K_d (ETS), A and B are concentrations of U3 MINI (M) and ETS (M), respectively, and $\min(A,B)$ is the lowest value of either A or B.

Hybridization rate constants of the U3–ETS duplex

Hybridization rate constants of the U3–ETS duplex were measured under equimolar concentrations of donor and acceptor (i.e., equimolar substrate concentrations). In the presence of protein, 10, 25, and 50 nM equimolar substrate concentrations were used for the assay; in the absence of protein, 1, 2, 5, 25, and 50 nM equimolar substrate concentrations were used. Ten-fold concentrated Rh-ETS

was added to Fl-U3 MINI with either saturating amounts of Imp3p and Imp4p or their buffers with no protein such that the final concentrations of substrates are equal. As with the determination of k_{on} (18S) (above), the ssFRET-dependent Fl quenching was converted into the appearance of [AB]$_{apparent}$ using Eq. (1) and fit to Eq. (2a) to determine k_{on} (ETS).

To ascertain that the fluorophores did not interfere with activity, we determined k_{on} (ETS) using 10 nM Fl-ETS-Rh and using substrates in which the donor and acceptor labels on the two RNA substrates were exchanged.

Estimation of errors

All equations were fit using least squares by PRISM5. The mean and standard deviation reported for the kinetic and thermodynamic values were calculated from at least three measurements.

Supplementary Data

Supplementary data associated with this article can be found, in the online version, at doi:10.1016/j.jmb.2009.05.072

References

1. Herschlag, D. (1995). RNA chaperones and the RNA folding problem. *J. Biol. Chem.* **270**, 20871–20874.
2. Granneman, S. & Baserga, S. J. (2004). Ribosome biogenesis: of knobs and RNA processing. *Exp. Cell Res.* **296**, 43–50.
3. Henras, A. K., Soudet, J., Gerus, M., Lebaron, S., Caizergues-Ferrer, M., Mougin, A. & Henry, Y. (2008). The post-transcriptional steps of eukaryotic ribosome biogenesis. *Cell. Mol. Life Sci.* **65**, 2334–2359.
4. Staley, J. P. & Woolford, J. L., Jr. (2009). Assembly of ribosomes and spliceosomes: complex ribonucleoprotein machines. *Curr. Opin. Cell Biol.* **21**, 109–118.
5. Oskarsson, T. & Trumpp, A. (2005). The Myc trilogy: lord of RNA polymerases [comment]. *Nat. Cell Biol.* **7**, 215–217.
6. Hughes, J. M. & Ares, M., Jr. (1991). Depletion of U3 small nucleolar RNA inhibits cleavage in the 5′ external transcribed spacer of yeast pre-ribosomal RNA and impairs formation of 18S ribosomal RNA. *EMBO J.* **10**, 4231–4239.
7. Beltrame, M. & Tollervey, D. (1992). Identification and functional analysis of two U3 binding sites on yeast pre-ribosomal RNA. *EMBO J.* **11**, 1531–1542.
8. Beltrame, M. & Tollervey, D. (1995). Base pairing between U3 and the pre-ribosomal RNA is required for 18S rRNA synthesis. *EMBO J.* **14**, 4350–4356.

9. Beltrame, M., Henry, Y. & Tollervey, D. (1994). Mutational analysis of an essential binding site for the U3 snoRNA in the 5′ external transcribed spacer of yeast pre-rRNA. *Nucleic Acids Res.* **22**, 5139–5147.

10. Hughes, J. M. (1996). Functional base-pairing interaction between highly conserved elements of U3 small nucleolar RNA and the small ribosomal subunit RNA. *J. Mol. Biol.* **259**, 645–654.

11. Sharma, K. & Tollervey, D. (1999). Base pairing between U3 small nucleolar RNA and the 5′ end of 18S rRNA is required for pre-rRNA processing. *Mol. Cell. Biol.* **19**, 6012–6019.

12. Dragon, F., Gallagher, J. E., Compagnone-Post, P. A., Mitchell, B. M., Porwancher, K. A., Wehner, K. A. *et al.* (2002). A large nucleolar U3 ribonucleoprotein required for 18S ribosomal RNA biogenesis. *Nature*, **417**, 967–970.

13. Grandi, P., Rybin, V., Bassler, J., Petfalski, E., Strauss, D., Marzioch, M. *et al.* (2002). 90S pre-ribosomes include the 35S pre-rRNA, the U3 snoRNP, and 40S subunit processing factors but predominantly lack 60S synthesis factors. *Mol. Cell*, **10**, 105–115.

14. Schafer, T., Strauss, D., Petfalski, E., Tollervey, D. & Hurt, E. (2003). The path from nucleolar 90S to cytoplasmic 40S pre-ribosomes. *EMBO J.* **22**, 1370–1380.

15. Osheim, Y. N., French, S. L., Keck, K. M., Champion, E. A., Spasov, K., Dragon, F. *et al.* (2004). Pre-18S ribosomal RNA is structurally compacted into the SSU processome prior to being cleaved from nascent transcripts in *Saccharomyces cerevisiae*. *Mol. Cell*, **16**, 943–954.

16. Gerczei, T. & Correll, C. C. (2004). Imp3p and Imp4p mediate formation of essential U3–precursor rRNA (pre-rRNA) duplexes, possibly to recruit the small subunit processome to the pre-rRNA. *Proc. Natl Acad. Sci. USA*, **101**, 15301–15306.

17. Lee, S. J. & Baserga, S. J. (1999). Imp3p and Imp4p, two specific components of the U3 small nucleolar ribonucleoprotein that are essential for pre-18S rRNA processing. *Mol. Cell. Biol.* **19**, 5441–5452.

18. Borovjagin, A. V. & Gerbi, S. A. (1999). U3 small nucleolar RNA is essential for cleavage at sites 1, 2 and 3 in pre-rRNA and determines which rRNA processing pathway is taken in *Xenopus* oocytes. *J. Mol. Biol.* **286**, 1347–1363.

19. Borovjagin, A. V. & Gerbi, S. A. (2000). The spacing between functional *cis*-elements of U3 snoRNA is critical for rRNA processing. *J. Mol. Biol.* **300**, 57–74.

20. Borovjagin, A. V. & Gerbi, S. A. (2004). *Xenopus* U3 snoRNA docks on pre-rRNA through a novel base-pairing interaction. *RNA*, **10**, 942–953.

21. Granneman, S., Gallagher, J. E., Vogelzangs, J., Horstman, W., van Venrooij, W. J., Baserga, S. J. & Pruijn, G. J. (2003). The human Imp3 and Imp4 proteins form a ternary complex with hMpp10, which only interacts with the U3 snoRNA in 60–80S ribonucleoprotein complexes. *Nucleic Acids Res.* **31**, 1877–1887.

22. Wehner, K. A., Gallagher, J. E. & Baserga, S. J. (2002). Components of an interdependent unit within the SSU processome regulate and mediate its activity. *Mol. Cell. Biol.* **22**, 7258–7267.

23. Pereira, M. J., Harris, D. A., Rueda, D. & Walter, N. G. (2002). Reaction pathway of the *trans*-acting hepatitis delta virus ribozyme: a conformational change accompanies catalysis. *Biochemistry*, **41**, 730–740.

24. Rueda, D., Wick, K., McDowell, S. E. & Walter, N. G. (2003). Diffusely bound Mg^{2+} ions slightly reorient stems I and II of the hammerhead ribozyme to increase the probability of formation of the catalytic core. *Biochemistry*, **42**, 9924–9936.

25. Saenger, W. (1984). Principles of nucleic acid structure. In *Springer Advanced Texts in Chemistry* (Cantor, C. R., ed.), Springer-Verlag New York, Inc., New York, NY.

26. Porschke, D. & Eigen, M. (1971). Co-operative non-enzymic base recognition: 3. Kinetics of the helix-coil transition of the oligoribouridylic–oligoriboadenylic acid system and of oligoriboadenylic acid alone at acidic pH. *J. Mol. Biol.* **62**, 361–381.

27. Herschlag, D. & Cech, T. R. (1990). Catalysis of RNA cleavage by the *Tetrahymena thermophila* ribozyme: 1. Kinetic description of the reaction of an RNA substrate complementary to the active site. *Biochemistry*, **29**, 10159–10171.

28. Schwille, P., Oehlenschlager, F. & Walter, N. G. (1996). Quantitative hybridization kinetics of DNA probes to RNA in solution followed by diffusional fluorescence correlation analysis. *Biochemistry*, **35**, 10182–10193.

29. Berger, A. B., Cabal, G. G., Fabre, E., Duong, T., Buc, H., Nehrbass, U. *et al.* (2008). High-resolution statistical mapping reveals gene territories in live yeast. *Nat. Methods*, **5**, 1031–1037.

30. French, S. L., Osheim, Y. N., Cioci, F., Nomura, M. & Beyer, A. L. (2003). In exponentially growing *Saccharomyces cerevisiae* cells, rRNA synthesis is determined by the summed RNA polymerase I loading rate rather than by the number of active genes. *Mol. Cell. Biol.* **23**, 1558–1568.

31. Hughes, J. M., Konings, D. A. & Cesareni, G. (1987). The yeast homologue of U3 snRNA. *EMBO J.* **6**, 2145–2155.

32. Gerbi, S. A. & Bokinsky, G. (2004). Pre-ribosomal RNA processing in multicellular organisms. In *The Nucleolus* (Olson, M. O. J., ed.), pp. 170–198, Kluwer Academic/Plenum Publishers, New York, NY.

33. Bhaskaran, H. & Russell, R. (2007). Kinetic redistribution of native and misfolded RNAs by a DEAD-box chaperone. *Nature*, **449**, 1014–1018.

34. Clegg, R. M. (1992). Fluorescence resonance energy transfer and nucleic acids. *Methods Enzymol.* **211**, 353–388.

35. Brinkmann, U., Mattes, R. E. & Buckel, P. (1989). High-level expression of recombinant genes in *Escherichia coli* is dependent on the availability of the *dnaY* gene product. *Gene*, **85**, 109–114.

36. Breslauer, K. J. (1995). Extracting thermodynamic data from equilibrium melting curves for oligonucleotide order–disorder transitions. *Methods Enzymol.* **259**, 221–242.